Research Paper
Computational Methods for Differential Equations
http://cmde.tabrizu.ac.ir
Vol. *, No. *, *, pp. 1-16
DOI:10.22034/cmde.2026.67988.3259

Newton-multigrid method for nonlinear silicon problem with relaxing boundary conditions

Adriano Rodrigues De Melo[1,*], Marcio Augusto Villela Pinto[2], Sebastião Romero Franco[3] and Priscila Dombrovski Zen[4]

[1]Catarinense Federal Institute, BR-280, Araquari, 89245-000, Santa Catarina, Brazil.

[2]Department of Mechanical Engineering, Federal University of Paraná, Polytechnic Center, Curitiba, 81530-000, Paraná, Brazil.

[3]Department of Mathematics, State University of the Central West, Irati, 84505-677, Paraná, Brazil.

[4]Graduate Program in Numerical Methods in Engineering, Federal University of Paraná, Polytechnic Center, Curitiba, 81530-000, Paraná, Brazil.

Abstract

This paper introduces a Newton-multigrid (Newton-MG) method to efficiently solve a nonlinear heat transfer problem in a homogeneous silicon rod. The numerical model is constructed using the Finite Difference Method (FDM) with a Central Difference Scheme (CDS) for spatial discretization and the Crank-Nicolson method for temporal approximation. Newton's method is applied to linearize the discretized equations and a multigrid Correction Scheme (CS) is integrated to solve the resulting linear system. Computational experiments demonstrate that, regardless of the physical and numerical parameters, the apparent order of discretization error converges to its theoretical asymptotic order. Additionally, the Newton-MG method exhibits rapid convergence, requiring few linearization steps while achieving a favorable convergence factor. The efficiency gain relative to the singlegrid method increases with the degree of nonlinearity in the physical model. Our findings confirm that Newton-MG is a robust and computationally efficient alternative for nonlinear heat conduction problems.

Keywords. Convective heat transfer, Multigrid correction scheme, Semiconductor modeling, Time-stepping methods.

2010 Mathematics Subject Classification. 35F31, 65M55, 65M06, 80M20.

1. Introduction

Nonlinear heat transfer is a research subject with applications in various areas of science and engineering. Nonlinearity in these models may arise, among other reasons, because thermophysical properties, such as thermal conductivity and specific heat capacity, may depend on temperature [3, 19, 36, 49].

The multiple application contexts of nonlinear heat equations include the study of heat transfer in biological tissue [2, 4, 43], the modeling of the microchip manufacturing process in the semiconductor industry [38] and of Functionally Graded Materials (FGMs) used in the modern aerospace and nuclear industries [24, 25, 46], the analysis of temperature-constrained topology optimization applied in the field of power electronics [47], and many others [14, 21]. This mathematical model is even applied in modeling the traffic flow of automated vehicles [41].

Given the intrinsic complexity of nonlinear heat transfer problems, analytical solutions are typically limited to specific cases [9, 22, 23]. As a result, computational methods provide a more accessible and general approach to assess the behavior of systems governed by Partial Differential Equations (PDEs) with a high level of accuracy.

Among several research studies associated with the development of numerical techniques for computational solution of the nonlinear PDEs, we highlight the study by Filipolv et al. [11], which described a physical model of heat conduction in semiconductors, considering temperature dependent thermal conductivity and relaxing boundary conditions. The numerical solution developed by these authors used the Finite Difference Method (FDM) with linearization by Newton's method. Similarly, Zhang et al. [46] developed an algorithm based on the Space-Time Backward Substitution Method (STBSM) for nonlinear transient heat conduction in FGMs, also utilizing global Newton linearization.

Received: 03 July 2025; Accepted: 18 April 2026.
∗ Corresponding author. Email: adriano.melo@ifc.edu.br.

Investigating nonlinear time-fractional partial integro-differential equations, Ghoreyshi et al. [15] used the Finite Block Method (FBM) to handle irregular computational domains, while employing a quasilinearization technique to manage nonlinearity. According to these authors, this method has the advantages of easy implementation, high accuracy, reduced storage requirements, and unconditional stability [1, 16].

Multigrid (MG) methods, in turn, are among the most powerful techniques for formulating numerical schemes designed to computationally solve PDEs [7, 42]. Their efficiency has been proven through several studies and tested in a wide variety of applications [5, 12, 28, 32, 33, 37, 45]. The multigrid method combines the fact that many iterative techniques for linear systems (such as the Gauss-Seidel and Jacobi methods) work well in smoothing the high-frequency error components, with the fact that the low-frequency modes can be well approximated on coarser grids [30, 48]. For this reason, the method employs a hierarchy of grids, where information is gone through between different levels using a combination of smoothing steps and an appropriate correction scheme.

When applied to nonlinear problems, multigrid methods can be associated with a linearization technique such as Picard iteration [33] or Newton's method [20], but can also be designed from the Full Approximation Scheme (FAS) approach [44, 45], which addresses nonlinearity directly. Comparing the performance of FAS and Newton-MG schemes applied to elliptical and parabolic problems discretized by finite elements, Brabazon et al. [6] observed that the Newton-MG method presented greater stability, as well as a shorter execution time. Additionally, Luo et al. [27] showed that these two strategies demonstrated good convergence properties when applied to solving incompressible poroelasticity equations with stress-dependent hydraulic conductivity. In the specific context of nonlinear heat conduction, we highlight the study by Zen et al. [45], who developed a numerical scheme through the multigrid FAS method integrating a Waveform Relaxation method (FAS-MGWR) for temporal sweep. Their numerical scheme was applied to the analysis of heat conduction in a silicon rod with relaxing boundary conditions, and demonstrated an excellent convergence factor and a high computational speed-up relative to its singlegrid version (singlegrid method).

In this work, we address heat conduction in a silicon rod through a methodology that employs time-stepping temporal sweep, as well as integrating Newton linearization and a multigrid correction scheme. By adding multigrid efficiency, we aim to improve the computational performance of Newton-based solvers in thermal modeling applications. The proposed methodology has the advantage of fast convergence due to the multigrid accelerator, which typically requires few iterations (MG cycles) and few linearizations. The time-stepping approach, classic in the treatment of transient problems, favors the use of MG (which is robust for elliptic problems [42]), since it results in an elliptic problem in each time step; however, it is limited in terms of parallelization. Although the MG method requires few linearizations, the extra calculations of the Jacobian matrix can increase algorithmic complexity. The FAS-MGWR approach overcomes these two limitations (parallelism and extra calculations with Jacobian), but in return requires a greater amount of computational memory [14]. Another limiting factor is stability, which, as we will see, the method is conditionally stable.

This paper is structured as follows: Section 2 introduces the physical model and details the development of the numerical approach for nonlinear heat conduction in a silicon rod with relaxing boundary conditions. Section 3 details the Newton-MG algorithm. Section 4 includes a code verification process, some metrics, and computational experiments designed to assess the quality and efficiency of the proposed numerical scheme. Finally, section 5 summarizes our main findings.

2. Mathematical and Computational Models

The mathematical model follows the formulation of Filipov et al. [11], considering a one-dimensional homogeneous silicon rod with temperature-dependent thermophysical properties. This study is essential for understanding thermal conduction in semiconductors, with direct applications in the manufacture of microchips, in the development of advanced materials and in technologies that require precise thermal control.

In general terms, consider a rod located on the x-axis between points a and b, laterally insulated and in thermal contact with a tank filled with liquid at a temperature $T(t)$, as shown in Fig. 1. In this material, the thermal conductivity is dependent on the temperature $u(x,t)$, making the mathematical model nonlinear.

The temperature in the tank is an exponentially relaxing function [11]:

$$T(t) = T_r + (T_0 - T_r)e^{-\frac{Q}{V}t}, \tag{2.1}$$

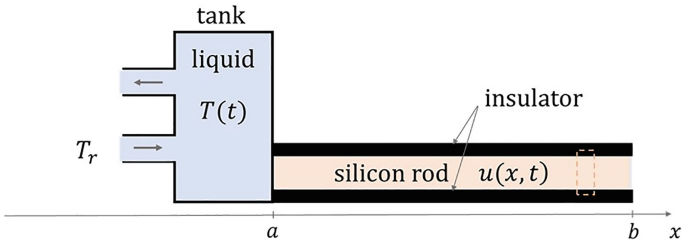

FIGURE 1. Physical model [11].

where V is the volume of the tank, T_0 is the temperature of the liquid in the tank at the initial time, T_r is the temperature of the incoming liquid and Q is the volume flow rate of both incoming and outgoing liquid.

2.1. **Nonlinear Heat Equation.** From the physical representation and the hypotheses described previously, Filipov et al. [11] deduced the following nonlinear PDE:

$$\rho c_p \frac{\partial u}{\partial t} = \frac{\partial}{\partial x}\left(\kappa(u)\frac{\partial u}{\partial x}\right), \quad x \in (a,b), \quad t > 0, \tag{2.2}$$

where $u(x,t)$ represents the temperature at position x at an instant t, while ρ refers to the density of silicon rod and c_p the heat capacity at constant pressure, which in the present model are both considered constant.

The thermal conductivity of silicon has an exponential dependence on temperature [26, 29] and therefore takes the following form [35, 36]:

$$\kappa(u) = \kappa_0 e^{\chi u}, \tag{2.3}$$

where κ_0 is the value of the thermal conductivity at a reference temperature and χ is the coefficient of temperature dependence associated with κ.

To complete the model, we add the initial condition:

$$u(x,0) = u_0(x), \quad x \in [a,b], \tag{2.4}$$

and the boundary conditions:

$$-\kappa\left(u(x,t)\right)\left.\frac{\partial u(x,t)}{\partial x}\right|_{x=a} = c\left(T(t) - u(a,t)\right) \quad \text{and} \quad u(b,t) = \beta, \quad t > 0, \tag{2.5}$$

where c is the mean convective heat transfer coefficient and $T(t)$ is the temperature in the tank given by Eq. (2.1).

The left part of Eq. (2.5), called the convective boundary condition, is obtained by equating the energy fluxes at $x = a$ expressed in the tank and the silicon rod. It is valid for solid-liquid contact surfaces, where the heat transport mechanisms are mainly due to convection in the liquid system [11, 45]. On the right-hand side of the same equation (at $x = b$), we have a Dirichlet boundary condition.

2.2. **Numerical Model.** Computational methods are essential tools for solving important problems such as the one described in the previous section, whose analytical solution is difficult to access or even non-existent. To proceed, we use the chain rule to differentiate $\partial\kappa(u)/\partial u = \chi\kappa(u)$ in Eq. (2.3), in order to rewrite Eq. (2.2) as

$$\rho c_p \frac{\partial u}{\partial t} = \chi\kappa(u)\left(\frac{\partial u}{\partial x}\right)^2 + \kappa(u)\frac{\partial^2 u}{\partial x^2}, \quad x \in (a,b), \quad t > 0. \tag{2.6}$$

The numerical model is developed on a spatial mesh of the form:

$$\Omega^h = \{x_i \in [a,b];\ x_i = a + (i-1)h,\ 1 \le i \le n_x\}, \tag{2.7}$$

where n_x is the number of discretization points and $h = (b-a)/(n_x - 1)$ is the spatial increment. Similarly, we define a temporal mesh of the form $t_n = (n-1)\tau \in (0,\ t_f]$, $2 \le n \le n_t$, where $\tau = t_f/(n_t - 1)$ is the time step, t_f is the final time and n_t is the number of time steps.

For the temporal approximation, we use the Crank-Nicolson (CN) method, while for the spatial approximation we use the FDM with second-order Central Difference Scheme (CDS), which leads to the following discretized form of Eq. (2.6):

$$\frac{\rho c_p}{\tau}\left(u_i^n - u_i^{n-1}\right) = \frac{\phi_i(\mathbf{u}^n)}{h^2} + \frac{\phi_i(\mathbf{u}^{n-1})}{h^2}, \quad 1 < i < n_x, \tag{2.8}$$

where n represents the current time step, $u_i^n = u(x_i, t_n)$, $\mathbf{u}^n = [u_1^n, \cdots, u_i^n, \cdots, u_{n_x}^n]^T$ and

$$\phi_i(\mathbf{u}^n) = \frac{\kappa\left(u_i^n\right)}{2}\left[\frac{\chi}{4}\left(u_{i+1}^n - u_{i-1}^n\right)^2 + u_{i+1}^n - 2u_i^n + u_{i-1}^n\right]. \tag{2.9}$$

For the left contour, i.e., for $i = 1$, we use CDS in Eq. (2.5) and obtain the following discretized form:

$$-\kappa\left(u_1^n\right)\left(\frac{u_2^n - u_0^n}{2h}\right) = c\left(T^n - u_1^n\right), \tag{2.10}$$

which can be rewritten as:

$$u_0^n = u_2^n + \frac{2hc\left(T^n - u_1^n\right)}{\kappa\left(u_1^n\right)}, \quad 1 \le n \le n_t. \tag{2.11}$$

Substituting Eq. (2.11) into Eq. (2.8), taking $i = 1$, we obtain:

$$\begin{aligned}\frac{\rho c_p}{\tau}\left(u_1^n - u_1^{n-1}\right) = {} & \frac{\chi c^2\left(T^n - u_1^n\right)^2}{2\kappa\left(u_1^n\right)} + \frac{\kappa\left(u_1^n\right)}{h^2}\left(u_2^n - u_1^n\right) + \frac{c\left(T^n - u_1^n\right)}{h} + \frac{\chi c^2\left(T^{n-1} - u_1^{n-1}\right)^2}{2\kappa\left(u_1^{n-1}\right)} \\ & + \frac{\kappa\left(u_1^{n-1}\right)}{h^2}\left(u_2^{n-1} - u_1^{n-1}\right) + \frac{c\left(T^{n-1} - u_1^{n-1}\right)}{h}, \quad 2 \le n \le n_t.\end{aligned} \tag{2.12}$$

Thus, Eqs. (2.8) and (2.12) constitute a nonlinear system that will be solved numerically by Newton's method. To do this, we introduce the vector $\mathbf{G}^n = [G_1^n, \cdots, G_i^n, \cdots, G_{n_x}^n]^T$, $2 \le n \le n_t$, as:

$$\begin{aligned}G_1^n = {} & \frac{\rho c_p}{\tau}\left(u_1^n - u_1^{n-1}\right) - \frac{\chi c^2\left(T^n - u_1^n\right)^2}{2\kappa\left(u_1^n\right)} - \frac{\kappa\left(u_1^n\right)}{h^2}\left(u_2^n - u_1^n\right) - \frac{c\left(T^n - u_1^n\right)}{h} \\ & - \frac{\chi c^2\left(T^{n-1} - u_1^{n-1}\right)^2}{2\kappa\left(u_1^{n-1}\right)} - \frac{\kappa\left(u_1^{n-1}\right)}{h^2}\left(u_2^{n-1} - u_1^{n-1}\right) - \frac{c\left(T^{n-1} - u_1^{n-1}\right)}{h},\end{aligned} \tag{2.13}$$

$$G_i^n = \frac{\rho c_p}{\tau}\left(u_i^n - u_i^{n-1}\right) - \frac{\phi_i(\mathbf{u}^n)}{h^2} - \frac{\phi_i(\mathbf{u}^{n-1})}{h^2}, \quad 2 \le i \le n_x - 1, \tag{2.14}$$

$$G_{n_x}^n = u_{n_x}^n - \beta. \tag{2.15}$$

The complete nonlinear system can be rewritten as $\mathbf{G}^n(\mathbf{u}^n) = \mathbf{0}$, $2 \le n \le n_t$, where $\mathbf{0}$ is the n_x-dimensional null vector. Newton iterations are then computed, starting from an initial guess $\mathbf{u}^{n,0}$, as follows:

$$\mathbf{u}^{n,\nu+1} = \mathbf{u}^{n,\nu} - \left(\mathbf{J}^{n,\nu}\right)^{-1}\mathbf{G}^{n,\nu}\left(\mathbf{u}^{n,\nu}\right), \quad \nu \ge 0, \quad 2 \le n \le n_t, \tag{2.16}$$

where

$$\mathbf{J}^{n,\nu} = \frac{\partial \mathbf{G}^n}{\partial \mathbf{u}^n}\left(\mathbf{u}^{n,\nu}\right), \quad \nu \ge 0, \quad 2 \le n \le n_t, \tag{2.17}$$

and ν represents the linearization step.

As a result, the nonzero elements of the Jacobian matrix $\mathbf{J}^{n,\nu}$, Eq. (2.17), valid for $2 \leq n \leq n_t$, $\nu \geq 0$ and $2 \leq i \leq n_x - 1$, are:

$$J_{i,i-1}^{n,\nu} = -\frac{1}{h^2}\frac{\partial \phi_i}{\partial u_{i-1}^{n,\nu}} = \frac{\kappa\left(u_i^{n,\nu}\right)}{2h^2}\left[\frac{\chi}{2}\left(u_{i+1}^{n,\nu} - u_{i-1}^{n,\nu}\right) - 1\right], \tag{2.18}$$

$$J_{i,i}^{n,\nu} = \frac{\rho c_p}{\tau} - \frac{1}{h^2}\frac{\partial \phi_i}{\partial u_i^{n,\nu}} = \frac{\rho c_p}{\tau} + \frac{\kappa\left(u_i^{n,\nu}\right)}{h^2} - \frac{\chi}{h^2}\phi_i(\mathbf{u}^n), \tag{2.19}$$

$$J_{i,i+1}^{n,\nu} = -\frac{1}{h^2}\frac{\partial \phi_i}{\partial u_{i+1}^{n,\nu}} = -\frac{\kappa\left(u_i^{n,\nu}\right)}{2h^2}\left[\frac{\chi}{2}\left(u_{i+1}^{n,\nu} - u_{i-1}^{n,\nu}\right) + 1\right], \tag{2.20}$$

whereas for $i = 1$, they are

$$J_{1,1}^{n,\nu} = \frac{\rho c_p}{\tau} + \frac{c}{h} + \frac{\chi c\left(T^n - u_1^{n,\nu}\right)}{\kappa\left(u_1^{n,\nu}\right)}\left[c + \frac{\chi c\left(T^n - u_1^{n,\nu}\right)}{2}\right] + \frac{\kappa\left(u_1^{n,\nu}\right)}{h^2}\left[1 - \chi\left(u_2^{n,\nu} - u_1^{n,\nu}\right)\right], \tag{2.21}$$

$$J_{1,2}^{n,\nu} = -\frac{\kappa\left(u_1^{n,\nu}\right)}{h^2}, \tag{2.22}$$

and when $i = n_x$, we have $J_{n_x,n_x}^{n,\nu} = 1$.

We set the initial guess to be $\mathbf{u}^{n,0} = \mathbf{u}^{n-1,\nu_c}$, where $\mathbf{u}^{n-1,\nu_c}$ is the solution from the previous time step converged after ν_c Newton linearization steps. In this respect, when $n = 2$ and $\nu = 0$, we use the initial condition given by Eq. (2.4).

2.3. **Stability Analysis.** We will prove stability by the energy method [15, 16]. Note, firstly, that the function ϕ, whose i-th component is represented in Eq. (2.9), is L-Lipschitz for every bounded open set, with constant $L > 0$ given according to the mean value inequality.

Theorem 2.1. *Let* $\mathbf{u}^n$ *be the approximate solution obtained by numerical scheme* (2.8). *If*

$$\frac{\tau L}{\rho c_p h^2} < 1, \tag{2.23}$$

then scheme (2.8) *is stable.*

Proof. Let $\mathbf{u}^n$ and $\mathbf{v}^n$ be numerical solutions computed by numerical scheme (2.8). Using $\mathbf{w}^n = \mathbf{u}^n - \mathbf{v}^n$ to represent the roundoff error equation, after appropriate substitutions, we produce the following equation:

$$\frac{\rho c_p}{\tau}\left(\mathbf{w}^n - \mathbf{w}^{n-1}\right) = \frac{\phi(\mathbf{u}^n) - \phi(\mathbf{v}^n)}{h^2} + \frac{\phi(\mathbf{u}^{n-1}) - \phi(\mathbf{v}^{n-1})}{h^2}. \tag{2.24}$$

Now, taking the inner product of Eq. (2.24) with $\mathbf{w}^n$, and applying the Cauchy-Schwarz inequality, we find:

$$\begin{aligned}\frac{\rho c_p}{\tau}\left\langle \mathbf{w}^n, \mathbf{w}^n\right\rangle - \frac{\rho c_p}{\tau}\left\langle \mathbf{w}^{n-1}, \mathbf{w}^n\right\rangle &= \frac{1}{h^2}\left\langle \phi(\mathbf{u}^n) - \phi(\mathbf{v}^n), \mathbf{w}^n\right\rangle + \frac{1}{h^2}\left\langle \phi(\mathbf{u}^{n-1}) - \phi(\mathbf{v}^{n-1}), \mathbf{w}^n\right\rangle, \\ &\leq \frac{1}{h^2}\left|\left|\phi(\mathbf{u}^n) - \phi(\mathbf{v}^n)\right|\right|\left|\left|\mathbf{w}^n\right|\right| + \frac{1}{h^2}\left|\left|\phi(\mathbf{u}^{n-1}) - \phi(\mathbf{v}^{n-1})\right|\right|\left|\left|\mathbf{w}^n\right|\right|.\end{aligned}$$

We again use the Cauchy-Schwarz inequality, as well as the Lipschitz continuity of ϕ, to reduce the last inequality to the following:

$$\begin{aligned}\frac{\rho c_p}{\tau}\left|\left|\mathbf{w}^n\right|\right|^2 &\leq \frac{\rho c_p}{\tau}\left\langle \mathbf{w}^{n-1}, \mathbf{w}^n\right\rangle + \frac{L}{h^2}\left|\left|\mathbf{w}^n\right|\right|^2 + \frac{L}{h^2}\left|\left|\mathbf{w}^{n-1}\right|\right|\left|\left|\mathbf{w}^n\right|\right|, \\ &\leq \frac{\rho c_p}{\tau}\left|\left|\mathbf{w}^{n-1}\right|\right|\left|\left|\mathbf{w}^n\right|\right| + \frac{L}{h^2}\left|\left|\mathbf{w}^n\right|\right|^2 + \frac{L}{h^2}\left|\left|\mathbf{w}^{n-1}\right|\right|\left|\left|\mathbf{w}^n\right|\right|.\end{aligned} \tag{2.25}$$

Next, we group similar terms to obtain:

$$\left(\frac{\rho c_p}{\tau} - \frac{L}{h^2}\right)\left|\left|\mathbf{w}^n\right|\right| \leq \left(\frac{\rho c_p}{\tau} + \frac{L}{h^2}\right)\left|\left|\mathbf{w}^{n-1}\right|\right|. \tag{2.26}$$

Using the hypothesis of the Theorem, we finally arrive at the desired result:

$$||\mathbf{w}^n|| \leq C^n \left|\left|\mathbf{w}^0\right|\right|, \quad \text{where} \quad C = \frac{\frac{\rho c_p}{\tau} + \frac{L}{h^2}}{\frac{\rho c_p}{\tau} - \frac{L}{h^2}} > 0. \tag{2.27}$$

□

3. Newton-MG Solver

Solving the linear system given by Eq. (2.16) provides a number of challenges. Direct methods for solving sparse systems may become impractical due to the high computational cost associated with the inversion of the matrix $\mathbf{J}^{n,\nu}$ [17]. For this reason, iterative methods, such as the Jacobi and the Gauss-Seidel method, are often preferred due to their efficiency in terms of computational cost and storage [8]. However, for highly refined meshes, these iterative methods tend to converge at a slow rate [10].

The multigrid method emerges as a powerful iterative technique designed for the efficient solution of large and sparse linear systems obtained from the discretization of PDEs [13, 34, 42]. It is constituted from the definition of a hierarchy of grids, where information circulates through restriction operators I_h^H, which transfer information from the fine grid Ω^h to the immediately coarser grid Ω^H, and prolongation operators I_H^h, which transfer information from the coarse grid Ω^H to the immediately finer grid Ω^h. The most common way to obtain grid Ω^H, called the standard coarsening strategy, is to double the spacing of grid Ω^h in all directions [42]. In this case, we say that a coarsening ratio (cr) equal to 2, that is, $H = 2h$.

As for the desired numerical solution, it is calculated on the finest grid, while on the coarser grids, where the smoothers are more efficient, correction estimates are calculated. The number of smoothings that will precede the restriction and prolongation operators are designated by ν_1 (number of pre-smoothings) and ν_2 (number of post-smoothings), while the way in which the grids are visited is called a cycle. In this work, we use V-cycles, also denoted by $V(\nu_1, \nu_2)$ [7, 42, 48].

Corrections can be performed in two possible ways. The Correction Scheme (CS), which uses only the residual in the correction process and is indicated for linear problems. The Full Approximation Scheme (FAS), in turn, is more appropriate for nonlinear problems and uses both the residual and the approximate solution in its correction strategy [7, 42]. In the context of nonlinear problems, we can also highlight two main approaches [18]. The first approach, the FAS scheme, incorporates the multigrid method concept directly into nonlinear problems. An algorithm derived by this technique was developed by Zen et al. [45]. The second approach, on the other hand, consists of performing a global linearization and then applying the CS scheme.

In this paper we propose the use of Newton linearization and therefore the CS scheme will be used. Furthermore, we will use V-cycles. Algorithm 1 describes the CS scheme with V-cycle and standard coarsening ratio ($cr = 2$), for solving a linear system at the l grid level.

In this work we adopted the Newton-MG method with time-stepping temporal sweep, as detailed in Algorithm 2.

The main part of Algorithm 2 is the linearization process developed in the previous section. Note that to incorporate the multigrid concept from Algorithm 1, we consider $\mathbf{e}^{n,\nu+1} = \mathbf{u}^{n,\nu+1} - \mathbf{u}^{n,\nu}$, so that Eq. (2.16) becomes:

$$\mathbf{J}^{n,\nu}\mathbf{e}^{n,\nu+1} = -\mathbf{G}^{n,\nu}\left(\mathbf{u}^{n,\nu}\right), \quad 2 \leq n \leq n_t, \quad \nu \geq 0. \tag{3.1}$$

Note that the Newton-MG Algorithm is structured as a time advance scheme in which, at each time step n, the approximation $\mathbf{u}^{n,\nu+1}$ is updated from the deviation $\mathbf{e}^{n,\nu+1}$.

4. Results and Discussions

In this section we address the numerical experiments designed to evaluate the numerical scheme and the code implemented for solving a nonlinear heat transfer problem in a silicon rod in thermal contact with a liquid medium.

The values of the physical parameters adopted in the experiments follow Filipov et al. [11], considering a thin and homogeneous rod in the interval $x \in [1, 3]$, excluding heat and radiation sources, with convective relaxing boundary conditions at $x = 1$ and unitary Dirichlet boundary conditions at $x = 3$, that is, $u(3, t) = 1$, according to Eq. (2.5),

Algorithm 1 MG(l).

Require: Input data, initial and boundary conditions;
while Stopping criterion is not reached **do**
  if $l = L_{\max}$ **then**
    Solve the system: $\mathbf{A}^{lh}\mathbf{v}^{lh} = \mathbf{f}^{lh}$ on the coarse grid $\Omega^{2^l h}$
  else
    Smooth ν_1 times $\mathbf{A}^{lh}\mathbf{v}^{lh} = \mathbf{f}^{lh}$ on the grid $\Omega^{2^l h}$
    Compute the defect $\mathbf{r}^{lh} = \mathbf{f}^{lh} - \mathbf{A}^{lh}\mathbf{v}^{lh}$ on the grid $\Omega^{2^l h}$
    Restrict the defect $\mathbf{f}^{(l+1)h} = I_{2^l h}^{2^{l+1}h}\mathbf{r}^{lh}$ from grid $\Omega^{2^l h}$ to grid $\Omega^{2^{l+1}h}$
    Solve at the next level: $\mathbf{MG}(l+1)$
    Interpolate and correct the approximation: $\mathbf{v}^{lh} \leftarrow \mathbf{v}^{lh} + I_{2^{l+1}h}^{2^l h}\mathbf{v}^{(l+1)h}$
    Smooth ν_2 times $\mathbf{A}^{lh}\mathbf{v}^{lh} = \mathbf{f}^{lh}$ on the grid $\Omega^{2^l h}$
  end if
end while

Algorithm 2 Newton-MG(n).

while Stopping criterion is not reached **do**
  Set $\mathbf{A}^h = \mathbf{J}^{n,\nu}$, $\mathbf{v}^h = \mathbf{0}$, $\mathbf{f}^h = \mathbf{G}^{n,\nu}\left(\mathbf{u}^{n,\nu}\right)$
  Solve the linear system using Algorithm 1: MG(1)
  Update $\mathbf{u}^{n,\nu+1} \leftarrow \mathbf{u}^{n,\nu} + \mathbf{v}^h$
  Compute $\mathbf{J}^{n,\nu+1}$ and $\mathbf{G}^{n,\nu+1}\left(\mathbf{u}^{n,\nu+1}\right)$
  Update $\nu \leftarrow \nu + 1$
end while

in addition to a unitary initial condition $u_0(x) = 1$. For the liquid containment system, $T_r = 2$, $T_0 = 1$, $Q = 1$ and $V = 1$. The density, heat capacity and mean convective heat transfer coefficient associated with silicon were fixed, respectively, at $\rho = 2.33$, $c_p = 0.7$ and $c = 0.1$ [11, 21]. Finally, the parameters κ_0 and χ were varied.

The source code was implemented in the Fortran language with the Intel® Fortran compiler, using double precision, and it runs on an operating system equipped with an Intel® Core™ i5-7200U processor, featuring a central processing unit (CPU) operating at 2.50 GHz and 16 GB of RAM.

For the stopping criterion associated with multigrid cycles, we adopted the infinite norm of the dimensionless residual of the k-th iteration with respect to the initial estimate, according to a tolerance ε_{MG}:

$$\frac{||\mathbf{r}^k||_\infty}{||\mathbf{r}^0||_\infty} < \varepsilon_{MG} = 10^{-10}, \quad k \geq 1. \tag{4.1}$$

Regarding the stopping criterion associated with linearizations, we use an estimate of the relative error calculated at the infinite norm applied to the increment corresponding to consecutive linearizations, divided by the current approximation and subject to a tolerance ε_{Lin}, that is,

$$\frac{||\mathbf{u}^{n,\nu} - \mathbf{u}^{n,\nu-1}||_\infty}{||\mathbf{u}^{n,\nu}||_\infty} < \varepsilon_{Lin} = 10^{-10}, \quad \nu \geq 1. \tag{4.2}$$

The multigrid and singlegrid methods were both implemented using the Gauss-Seidel solver with red-black ordering. With the exception of section 4.2, we used spatial and temporal meshes spacings of the same size ($h = \tau$) and, in addition, the other multigrid configurations were: cycles of type $V(1,1)$; standard coarsening ($cr = 2$); full weighting operator I_h^{2h} (restriction) and linear interpolation operator I_{2h}^h (prolongation).

4.1. **Code Verification.** Initially, we evaluated the algorithm through code verification. This phase involved both qualitative and quantitative analyses.

In the first analysis, we compared the numerical solutions produced by the algorithm developed by Filipov et al. [11] and those derived from our singlegrid and multigrid algorithms. The κ_0 and χ parameters were varied by 0.5 and 0.1, respectively, while the other physical and numerical parameters were those previously stated.

Figure 2 shows the solutions computed by the three numerical schemes: our SG (singlegrid) and MG (multigrid) implementations and the Reference Solution (RS), the latter produced by the code implemented and kindly provided by Filipov et al. [11]. From this experiment, it is possible to observe a good agreement between the reference solutions [11] and those produced by the proposed algorithm. This confirms the reliability of the implemented code.

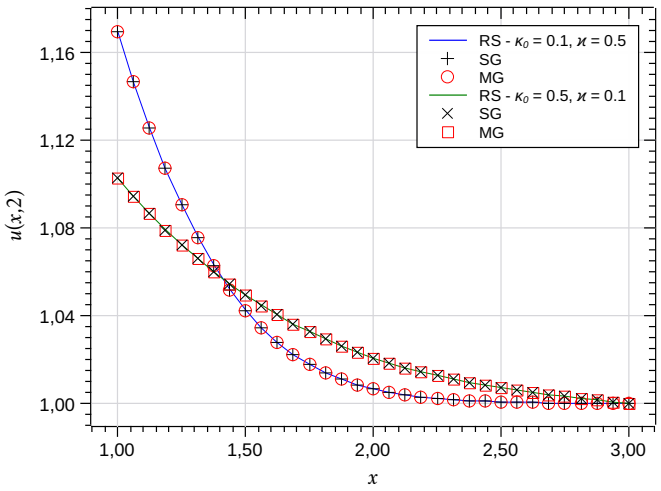

FIGURE 2. Comparison between solutions.

To proceed with the second part of the code verification, we will calculate the apparent order p_U of discretization error of the numerical approximation. This metric is indicated when a analytical solution is not known [39]. With the apparent order it is possible to verify whether the order of a numerical solution tends to the asymptotic order p_L of discretization error, as the mesh spacing h is reduced. It can be calculated as follows [45]:

$$p_U = \frac{\log\left|\dfrac{\phi_2 - \phi_3}{\phi_1 - \phi_2}\right|}{\log(q)}, \tag{4.3}$$

where ϕ_1, ϕ_2 and ϕ_3 are numerical approximations calculated on three meshes of different sizes, called fine, coarse and super-coarse, with respective spacings h_1, h_2 and h_3, and having a refinement ratio $q = h_3/h_2 = h_2/h_1$. In this work, we are using $q = cr = 2$.

Note that the asymptotic order of the proposed numerical scheme must be $p_L = 2$, since the spatial and temporal discretizations are, respectively, CDS and Crank-Nicolson method, both second order. Furthermore, we adopted two criteria used only in this test: in addition to adopting quadruple precision, the iterations determined by Eqs. (4.1) and (4.2) were performed until the rounding error was reached. This approach seeks to isolate the effects of discretization error, in order to minimize other sources of error.

Figure 3 shows a graphical representation of the test implemented for the variables of interest: average temperature (u_m), temperature at the center of the domain (u_c) and temperature at the left boundary (u_a), all calculated in the last time step, considering the same combinations of κ_0 and χ used in the previous qualitative analysis. As expected from the previous discussion, regardless of the choice of parameters κ_0 and χ, the apparent order p_U tends to the asymptotic order $p_L = 2$ as the mesh is refined.

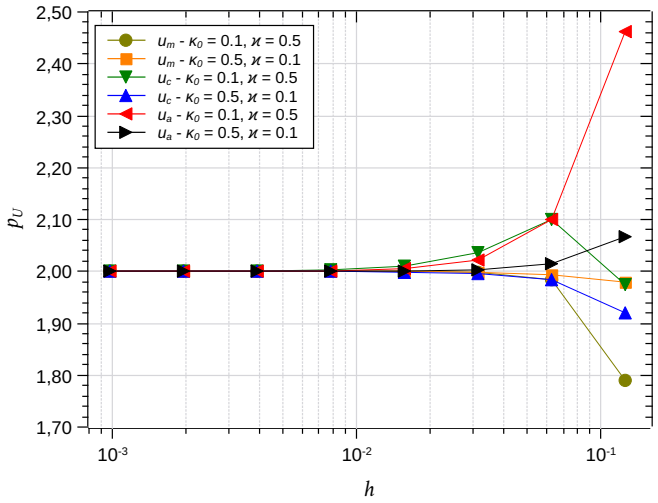

FIGURE 3. Apparent order p_U of discretization error of the numerical solutions for the variables u_m (average temperature), u_c (temperature at the central point) and u_a (temperature at the left contour), calculated in the last time step.

4.2. **Numerical Stability.** Our numerical experiments corroborate the stability condition of Theorem 2.1. An abrupt change in the temperature profile can generate non-physical oscillations. We simulated this phenomenon by altering the data that define the temperature T of the liquid, setting $T_r = 75$ and $T_0 = 74$ (the other parameters described at the beginning of Section 4 were kept the same). This configuration results in a relatively high temperature variation on the left boundary. Figure 4 shows the behavior of the numerical solution calculated at this point ($x = a$), considering two mesh configurations: the first Ω_1^h, with $\tau = h$, and the second Ω_2^h satisfying condition (2.23). In this comparison, we include the reference solution (RS) calculated on a super-refined mesh. The numerical solution is free of oscillations, provided the stability condition is met, as shown by the numerical solutions in meshes Ω_1^h and Ω_2^h.

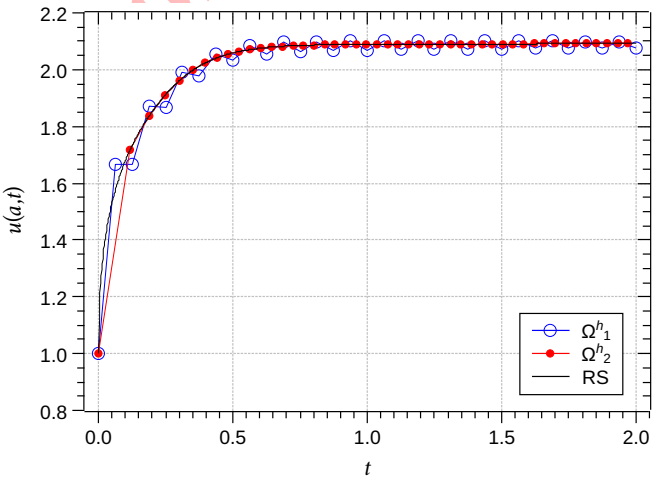

FIGURE 4. Numerical solution on the left boundary, computed on meshes Ω_1^h and Ω_2^h.

When the underlying solution is sufficiently smooth (without abrupt variations), the numerical solution does not exhibit oscillation (as seen in the graphs in Figure 2). This remark is consistent with the fact that linear stability extends to the non-linear scenario, provided that the underlying solution involved is sufficiently smooth [40].

In this sense, Eq. (2.23) represents a measure of the degree of sensitivity of the proposed scheme in relation to the choice of initial and boundary conditions, as well as the physical parameters, since they interfere with the smoothness of the underlying solution involved.

4.3. **Numerical Results.** In this section, we present some metrics used to evaluate the efficiency and robustness of the Newton-MG method. Of the physical parameters presented at the beginning of Section 4, only κ_0 and χ are modified in order to take a range of values. Regarding the numerical model, we emphasize that we adopted $\varepsilon_{MG} = \varepsilon_{Lin} = 10^{-10}$ and $\tau = h$ (the physical settings of the present study resulted in a smooth numerical solution, such that condition (2.23) was not triggered in any case).

4.3.1. *Average Convergence Factor.* In this section, we present the average convergence factor, a metric commonly used to evaluate multigrid methods and represents the average reduction factor of the residual after a multigrid cycle. In this work, the average convergence factor ρ_M is calculated based on the arithmetic mean of the asymptotic convergence factor ρ_m^k [33]:

$$\rho_M = \frac{1}{n_t - 1}\sum_{j=2}^{n_t} \overline{\rho}_m^j, \quad \overline{\rho}_m^j = \frac{1}{it_{Lin}}\sum_{k=1}^{it_{Lin}} \rho_m^k, \quad \rho_m^k = \sqrt[it_{MG}]{\frac{||\mathbf{r}^{it_{MG}}||_\infty}{||\mathbf{r}^0||_\infty}}, \tag{4.4}$$

where it_{MG} is the number of MG cycles of the k-th linearization, it_{Lin} is the number of linearizations in the j-th time step, and n_t is the total number of time steps.

Remark 4.1. Note in Eq. (4.4) that ρ_M is sensitive to the iteration error of the MG cycles and the iteration error due to the linearization process, but is not affected by the order of convergence (order of discretization error $p_L = 2$), which is determined only by the underlying spatial and temporal discretizations.

Figure 5 shows the evolution of the average convergence factor ρ_M in terms of the number of unknowns $\mathbf{N} = (n_x - 1)(n_t - 1)$, calculated for different combinations of parameters κ_0 and χ, where $n_x = 2^{n_g} + 1$ is the number of spatial grid points, n_t is the number of points on the temporal axis assuming $n_t = n_x$ and n_g is the number of grids. MG methods are considered efficient when the average convergence factor is close to zero and, on the other hand, the closer it is to unity, the lower its efficiency [7]. We observe that ρ_M stabilizes to values below 0.102 as the grid is refined, regardless of the choice of physical parameters, indicating efficiency and robustness of the method.

To complement this analysis, we show in Table 1 the average number of Newton linearizations and the average number of MG cycles (in parentheses), considering the physical parameters (κ_0 and χ) and the discretization parameters (represented by grid number n_g) assuming different values. We can observe that the number of linearizations required is always small in all cases, regardless of the values of the physical and discretization parameters, which shows the robustness of the algorithm.

Table 1 also shows that the average number of MG cycles stabilizes below 11 average cycles as the grid is refined, regardless of the values of the physical parameters, which also indicates the robustness of the method.

Remark 4.2. The high value of the average number of MG cycles in the case where $\kappa_0 = 100.0$, $\chi = 0.5,\ 1.0,\ 2.0$ and $5 \leq n_g \leq 8$, is in agreement with what was observed during the analysis of the average convergence factor that is represented in Figure 5. In this range, ρ_M decreases from 0.338395 to 0.150725, indicating that a greater number of MG cycles (although decreasing in relation to the number of unknowns) are necessary to reduce the residual to the stopping criterion level.

In this sense, ρ_M calculated using Eq. (4.4) proved to be a good estimator of the average number of MG cycles. For example, in the case where $\kappa_0 = 100.0$, $\chi = 2.0$ and $n_g = 5$, we have $\rho_M = 0.338395$ and the average number of MG cycles to reach the tolerance of $\varepsilon_{MG} = 10^{-d} = 10^{-10}$ can be estimated by [7]:

$$\overline{it}_{MG} > \frac{-d}{\log(0.338395)} = \frac{-10}{\log(0.338395)} = 21.25055, \tag{4.5}$$

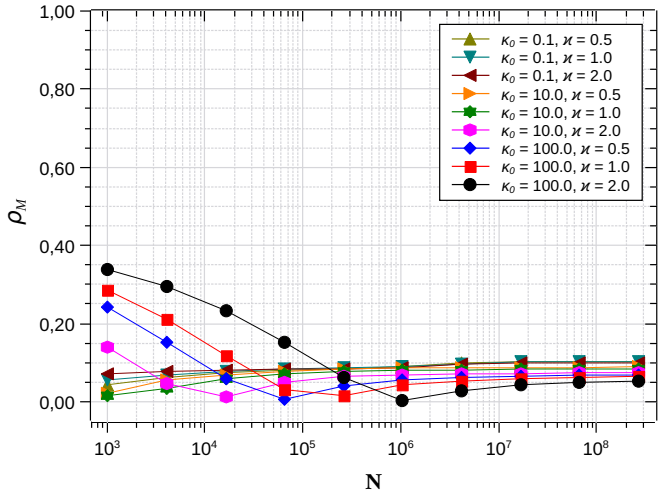

FIGURE 5. Average convergence factor ρ_M *versus* the number of unknowns **N**.

TABLE 1. Average number of linearization and MG cycles (in parentheses) for different number of grids n_g and different values for the physical parameters χ and κ_0.

	κ_0								
	0.1			10.0			100.0		
	χ								
n_g	0.5	1.0	2.0	0.5	1.0	2.0	0.5	1.0	2.0
5	3.0 (7.6)	3.0 (8.4)	3.0 (9.3)	3.0 (6.6)	3.0 (5.7)	3.0 (12.4)	2.6 (16.8)	2.6 (18.8)	2.3 (21.9)
6	3.0 (8.6)	3.0 (9.2)	3.0 (9.5)	3.0 (8.6)	3.0 (7.0)	2.9 (7.7)	2.2 (12.9)	2.2 (14.9)	2.0 (19.0)
7	3.0 (9.4)	3.0 (9.5)	3.0 (9.5)	2.8 (8.7)	2.8 (8.7)	2.5 (5.8)	2.0 (9.0)	2.0 (11.0)	2.0 (16.0)
8	3.0 (9.6)	3.0 (9.6)	3.0 (9.7)	2.4 (9.7)	2.3 (8.9)	2.1 (8.0)	2.0 (5.0)	2.0 (7.0)	2.0 (13.0)
9	3.0 (9.6)	3.0 (9.8)	3.0 (9.8)	2.0 (9.9)	2.0 (9.8)	2.0 (9.0)	2.0 (8.0)	2.0 (6.0)	2.0 (9.0)
10	2.8 (10.1)	2.8 (10.1)	2.8 (9.9)	2.0 (10.0)	2.0 (9.9)	2.0 (9.0)	2.0 (8.0)	2.0 (8.0)	2.0 (4.0)
11	2.1 (10.7)	2.3 (10.5)	2.1 (10.5)	2.0 (10.0)	2.0 (9.9)	2.0 (9.0)	2.0 (9.0)	2.0 (8.0)	2.0 (7.0)
12	2.0 (10.8)	2.0 (10.8)	2.0 (10.6)	2.0 (10.0)	2.0 (10.0)	2.0 (9.0)	2.0 (9.0)	2.0 (9.0)	2.0 (8.0)
13	2.0 (10.9)	2.0 (10.8)	2.0 (10.7)	2.0 (10.0)	2.0 (10.0)	2.0 (9.0)	2.0 (9.0)	2.0 (9.0)	2.0 (8.0)
14	2.0 (10.9)	2.0 (10.8)	2.0 (10.7)	2.0 (10.0)	2.0 (10.0)	2.0 (9.0)	2.0 (9.0)	2.0 (9.0)	2.0 (8.0)

a value very close to the 21.9 shown in Table 1.

4.3.2. *CPU Time, Complexity, and Speed-up.* In this section, we evaluate the performance of the multigrid method based on two concepts associated with processing time: the order of complexity and speed-up.

In Figure 6, on a bi-logarithmic scale, we show the CPU time in relation to the number of unknowns **N** corresponding to the multigrid and singlegrid methods. With this processing time data, we can obtain the order of complexity p of an algorithm from an exponential adjustment as [31, 32]:

$$\mathrm{t}_{CPU}(\mathbf{N}) = \gamma \mathbf{N}^p, \tag{4.6}$$

where **N** is the total number of unknowns and γ is a constant related to the method. The ideal context for multigrid methods is one in which the order of complexity p is close to unity and the parameter γ tends to zero, which means that the computational cost increases proportionally to the number of unknowns **N** [7, 42, 48].

In Table 2 we show the estimates of the order of complexity p and the parameter γ for the multigrid method and its single mesh version.

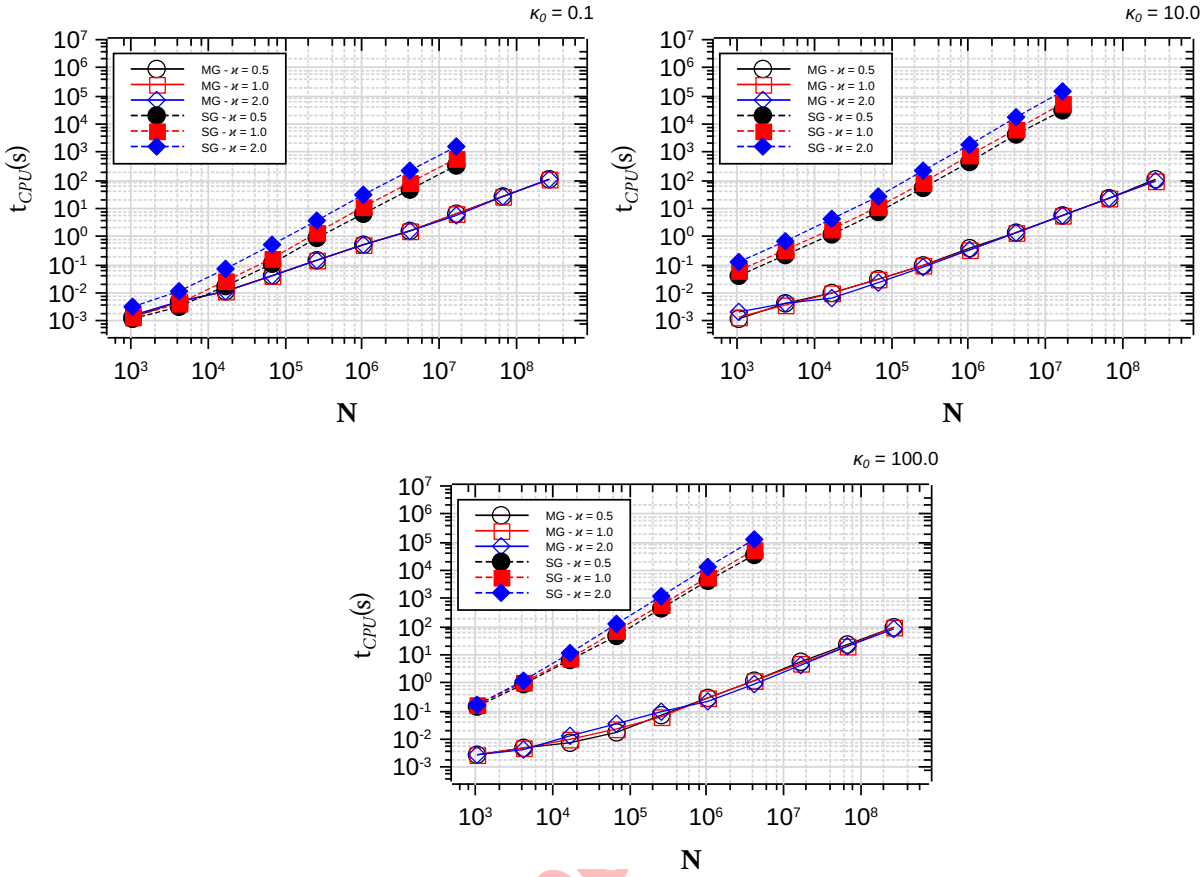

FIGURE 6. Computational time *versus* number of unknowns **N**, computed for different values of the physical parameters.

TABLE 2. Order of complexity estimated for the multigrid and singlegrid methods, computed for different values of the physical parameters.

		Singlegrid		Multigrid	
κ_0	χ	γ	p	γ	p
0.1	0.5	1.2848E-08	1.4450	2.3529E-07	1.0282
	1.0	3.7483E-08	1.4118	1.8235E-07	1.0415
	2.0	5.6502E-08	1.4475	3.7403E-07	1.0020
10.0	0.5	5.0284E-07	1.4955	7.6624E-08	1.0864
	1.0	6.9319E-07	1.5057	2.6190E-07	1.0175
	2.0	1.4976E-06	1.5190	2.7966E-07	1.0100
100.0	0.5	2.1721E-06	1.5469	2.3723E-07	1.0183
	1.0	1.3555E-06	1.6012	3.2310E-08	1.1257
	2.0	1.4925E-06	1.6542	2.2523E-07	1.0157

While the multigrid method presents values of the order of complexity p close to unity, regardless of the values attributed to the physical parameters, indicating its robustness and in agreement with the literature; the singlegrid method presents p with values greater than 1 and dependent on the configuration of the physical parameters, assuming

approximate values of 1.4, 1.5 and 1.6 for κ_0 equal to 0.1, 10.0 and 100.0, respectively. Regarding the parameter γ, we can see that all are close to zero, in agreement with the literature.

The data in Figure 6 also made it possible to calculate the speed-up S, used to evaluate the increase in execution speed of the multigrid method in relation to its singlegrid version. This metric is calculated as [45]:

$$S(\mathbf{N}) = \frac{\mathrm{t}_{CPU}^{SG}(\mathbf{N})}{\mathrm{t}_{CPU}^{MG}(\mathbf{N})}. \tag{4.7}$$

In Figure 7 we show a graphical representation of this speed-up metric calculated for different configurations of the physical parameters. Note that the gain in processing speed depends on the combination of parameters κ_0 and χ. For example, considering fixed $\mathbf{N} = 2048 \times 2048 = 4194304$ and $\chi = 0.5$, we observe an approximate speed-up of 29, 2700 and 30900, for κ_0 assuming values of 0.1, 10.0 and 100.0, respectively. This means, considering this last case, that the multigrid method is approximately 30900 times faster than its singlegrid counterpart. We can see an even more significant advantage of the multigrid method when we set $\kappa_0 = 100.0$ and $\chi = 2.0$, a configuration in which the calculated speed-up is approximately 140600. Furthermore, we highlight that the method becomes even more efficient for high nonlinearities.

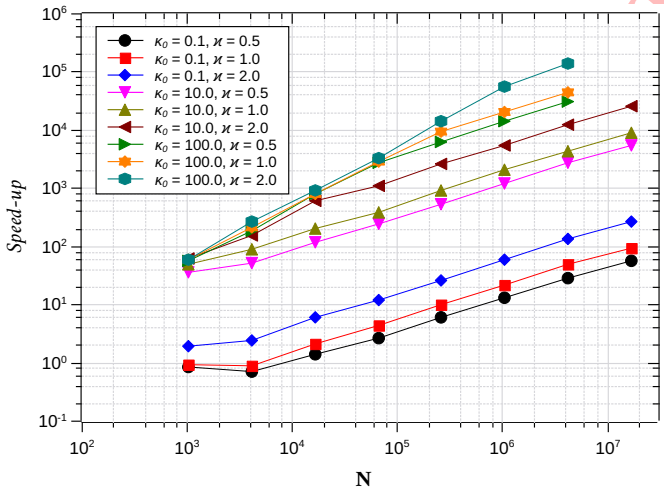

FIGURE 7. Speed-up calculated for different values of the physical parameters.

Finally, we observe an increasing pattern of the curves (Figure 7), indicating a growth in S as $\mathbf{N}$ grows, a highly desired property [45].

5. CONCLUSION

This study presents a Newton-MG method for solving one-dimensional nonlinear heat conduction in a silicon rod with relaxing boundary conditions. The numerical model employs the Crank-Nicolson method for temporal discretization and second-order FDM for spatial approximation, and is complete with Newton linearization and a CS multigrid. Code verification confirms strong agreement with benchmark solutions from the literature. The various numerical tests carried out under different scenarios establish the efficiency and robustness of the Newton-MG method to address non-linear thermal modeling problems, as they demonstrate: i) convergence factors close to those indicated in literature; ii) a low number of linearization; iii) efficient and reduced multigrid cycles; iv) computational complexity according to reference values; and v) significant speed-up compared to singlegrid methods. The methodology can be extended to broader applications in heat transfer modeling, semiconductor analysis, and nonlinear numerical simulations of the real world.

Acknowledgment

The authors extend their gratitude to researchers Stefan M. Filipov, István Faragó and Ana Avdzhieva for their generosity in providing their computational code, which allowed the code verification step to be carried out. To the Catarinense Federal Institute, for supporting the first author in his professional development. All authors would like to thank the Graduate Program in Numerical Methods in Engineering, Federal University of Paraná, Brazil. Finally, we thank the anonymous reviewers for helpful comments, which led to significant improvement in the manuscript.

References

[1] M. Abbaszadeh, A. Ghoreyshi, and M. Dehghan, *A finite block method framework for nonlinear fractional integro-differential equations*, Math. Methods Appl. Sci., (2025), 1–19.
[2] A. Andreozzi, L. Brunese, M. Iasiello, C. Tucci, and G. P. Vanoli, *Modeling heat transfer in tumors: A review of thermal therapies*, Ann. Biomed. Eng., *47*(3) (2019), 676–693.
[3] M. Becker, *Nonlinear transient heat conduction using similarity groups*, ASME. J. Heat Transfer, *122*(1) (2000), 33–39.
[4] A. Belmiloudi, *Parameter identification problems and analysis of the impact of porous media in biofluid heat transfer in biological tissues during thermal therapy*, Nonlinear Anal.: Real World Appl., *11*(3) (2010), 1345–1363.
[5] P. Benedusi, M. L. Minion, and R. Krause, *An experimental comparison of a space-time multigrid method with PFASST for a reaction-diffusion problem*, Comput. Math. Appl., *99* (2021), 162–170.
[6] K. J. Brabazon, M. E. Hubbard, and P. K. Jimack, *Nonlinear multigrid methods for second order differential operators with nonlinear diffusion coefficient*, Comput. Math. Appl., *68*(12, Part A) (2014), 1619–1634.
[7] W. L. Briggs, V. E. Henson, and S. F. McCormick, *A multigrid tutorial*, SIAM, Philadelphia, 2000.
[8] R. L. Burden, and J. D. Faires, *Numerical analysis*, Cengage Learning, Boston, 2011.
[9] A. Farina, and R. Gianni, *Self-similar solutions for the heat equation with a positive non-Lipschitz continuous, semilinear source term*, Nonlinear Anal.: Real World Appl., *79* (2024), 104121.
[10] R. P. Fedorenko, *A relaxation method for solving elliptic difference equations*, USSR Comput. Math. and Math. Phys., *1*(4) (1962), 1092–1096.
[11] S. M. Filipov, I. Faragó, and A. Avdzhieva, *Mathematical modelling of nonlinear heat conduction with relaxing boundary conditions*, in Numerical Methods and Applications, Springer, Cham, 2023, 146–158.
[12] S. R. Franco, F. J. Gaspar, M. A. V. Pinto, and C. Rodrigo, *Multigrid method based on a space-time approach with standard coarsening for parabolic problems*, Appl. Math. Comput., *317* (2018), 25–34.
[13] S. R. Franco, and M. A. V. Pinto, *A space-time multigrid method for poroelasticity equations with random hydraulic conductivity*, Numer. Heat Transf. B: Fundam., *85*(9) (2024), 1226–1235.
[14] F. J. Gaspar, and C. Rodrigo, *Multigrid waveform relaxation for the time-fractional heat equation*, SIAM J. Sci. Comput., *39*(4) (2017), 1201–1224.
[15] A. Ghoreyshi, M. Abbaszadeh, M. A. Zaky and M. Dehghan, *Finite block method for nonlinear time-fractional partial integro-differential equations: Stability, convergence, and numerical analysis*, Appl. Numer. Math., *214* (2025), 82–103.
[16] A. Ghoreyshi, M. Abbaszadeh, M. A. Zaky and M. Dehghan, *Two high-order numerical schemes based on the Lagrange polynomials for solving a distributed-order time-fractional partial integro-differential equation on non-rectangular domains*, J. Appl. Math. Comput., *71* (2025), 7271–7311.
[17] G. H. Golub, and C. Van Loan, *Matrix computations*, Johns Hopkins Press, Baltimore, 1996.
[18] V. E. Henson, *Multigrid methods nonlinear problems: an overview*, in Computational Imaging, 2003, 36–48.
[19] J.Y. Hristov, *Transient heat conduction with variable thermophysical properties power-law temperature-depenent heat capacity and thermal conductivity*, Therm. Sci., *27*(1) 2023), 441–422.
[20] H. Hu, M. Li, K. Pan, and P. Wu, *An extrapolation accelerated multiscale Newton-MG method for fourth-order compact discretizations of semilinear Poisson equations*. Comput. Math. Appl., *113* (2022), 189–197.
[21] F. P. Incropera, D. P. Dewitt, T. L. Bergman, and T. L. Lavine, *Fundamentals of heat and mass transfer*, John Wiley & Sons, NJ, 2006.

[22] A. Kazakov, L. Spevak, O. Nefedova, and A. Lempert, *On the analytical and numerical study of a two-dimensional nonlinear heat equation with a source term*, Symmetry, *12*(6) (2020).
[23] A. A. Kosov, and E. I. Semenov, *Reduction method and new exact solutions of the multidimensional nonlinear heat equation*, Diff. Equat., *58* (2022), 187–194.
[24] M. Li, M. Lei, A. Munjiza, and P. H. Wen, *Frictional contact analysis of functionally graded materials with Lagrange finite block method*, Int. J. Numer. Methods Eng., *103* (2015), 391–412.
[25] J. Li, J.Z. Liu, T. Korakianitis, and P.H. Wen, *Finite block method in fracture analysis with functionally graded materials*, Eng. Anal. Bound. Elem., *82* (2017), 57–67.
[26] J. Lienemann, A. Yousefi, and J. G. Korvink, *Nonlinear heat transfer modeling*, in Dimension reduction of Large-scale systems, Springer, Berlin, 2005, 327–331.
[27] P. Luo, C. Rodrigo, F. J. Gaspar, and C. W. Oosterlee, *Multigrid method for nonlinear poroelasticity equations*, Comput. Visual Sci., *17*(5) (2015), 255–265.
[28] M. F. Malacarne, M. A. V. Pinto, and S. R. Franco, *Performance of the multigrid method with time-stepping to solve 1D and 2D wave equations*, Int. J. Comput. Methods Eng. Sci. Mech., *23*(1) (2022), 45–56.
[29] P. D. Maycock, *Thermal conductivity of silicon, germanium, III-V compounds and III-V alloys*, Solid-State Electronics, *10*(3) (1967), 161–168.
[30] F. Oliveira, M. A. V. Pinto, C. H. Marchi and L. K. Araki, *Optimized partial semicoarsening multigrid algorithm for heat diffusion problems and anisotropic grids*, Appl. Math. Model., *36*(10) (2012), 4665–4676.
[31] F. D. Oliveira, S. R. Franco, and M. A. V. Pinto, *The effect of multigrid parameters in a 3D heat diffusion equation*, Int. J. Appl. Mech. Eng., *23*(1) (2018), 213–221.
[32] J. M. B. Oliveira, L. K. Araki, M. A. V. Pinto, and S. F. T. Gonçalves, *An alternative full multigrid SIMPLEC approach for the incompressible Navier-Stokes equations*. Numer. Heat Transf. B: Fundam., *83*(6) (2023), 410–432.
[33] M. L. Oliveira, M. A. V. Pinto, C. Rodrigo, and F. J. Gaspar, *Modified Picard with multigrid method for two-phase flow problems in rigid porous media*, Int. J. Numer. Methods Eng., *125*(5) (2024), 7397.
[34] M. A. V. Pinto, C. Rodrigo, F. J. Gaspar and C. W. Oosterlee, *On the robustness of ILU smoothers on triangular grids*, Appl. Numer. Math., *106* (2016), 37–52.
[35] M. Rencz, and V. Szekely, *Non-linearity issues in the dynamic compact model generation [package thermal modeling]*, in: Ninteenth annual IEEE semiconductor thermal measurement and management symposium, 2003, 263–270.
[36] M. Rencz, and V. Szekely, *Studies on the nonlinearity effects in dynamic compact model generation of packages*, IEEE Transactions on Components and Packaging Technologies, *27*(1) (2004), 124–130.
[37] C. D. Santiago, G. R. Ströher, M. A. V. Pinto, and S. R. Franco, *A multigrid waveform relaxation method for solving the Pennes bioheat equation*, Numer. Heat Transf.; A: Appl., *83*(9) (2023), 976–990.
[38] A. Schaum, S. Koch, M. Kleindienst, M. Reichhartinger, T. Meurer, J. A. Moreno, and M. Horn, *Observer design for a nonlinear heat equation: Application to semiconductor wafer processing*, J. Process Control, *119* (2022), 34–43.
[39] L. P. Silva, B. B. Rutyna, A. R. S. Righi, and M. A. V. Pinto, *High order of accuracy for Poisson equation obtained by grouping of repeated Richardson extrapolation with fourth order schemes*, CMES - Comput. Model. Eng. Sci., *128*(2) (2021), 699–715.
[40] E. Tadmor, *A review of numerical methods for nonlinear partial differential equations*, Bull. Amer. Math. Soc., *49*(4) (2012), 507–554.
[41] D. Theodosis, I. Karafyllis, G. Titakis, I. Papamichail, and M. Papageorgiou, *A nonlinear heat equation arising from automated-vehicle traffic flow models*, J. Comput. Appl. Math., *437* (2024), 115443.
[42] U. Trottenberg, C. Oosterlee, and A. Schüller, *Multigrid*, Academic Press, San Diego, 2001.
[43] C. Tucci, M. Trujillo, E. Berjano, M. Iasiello, A. Andreozzi, and G. P. Vanoli, *Pennes' bioheat equation vs. porous media approach in computer modeling of radiofrequency tumor ablation*, Sci. Rep., *11*(1) (2021), 5272.
[44] D. C. Zanatta, L. K. Araki, M. A. V. Pinto, and D. F. Moro, *Performance of geometric multigrid method for two-dimensional Burgers' equations with non-orthogonal, structured curvilinear grids*, CMES - Comput. Model. Eng. Sci., *125*(3) (2020), 1061–1081.

[45] P. D. Zen, M. A. V. Pinto, and S. R. Franco, *A multigrid waveform relaxation method for solving the nonlinear silicon problem with relaxing boundary conditions*, Numer. Heat Transf. B: Fundam., *86*(9) (2025), 3002–3017.
[46] Y. Zhang, T. Rabczuk, J. Lu, S. Lin, and J. Lin, *Space-time backward substitution method for nonlinear transient heat conduction problems in functionally graded materials*, Comput. Math. Appl., *124* (2022), 98–110.
[47] C. Zhuang, Z. Xiong, and H. Ding, *Temperature-constrained topology optimization of nonlinear heat conduction problems*, J. Comput. Des. Eng., *8*(4) (2021), 1059–1081.
[48] P. Wesseling, *An introduction to multigrid methods*. John Wiley & Sons, Chichester, 1992.
[49] K. Yang, H. Y. Li, H. F. Peng, and X. W. Gao, *New interface integration BEM for solving multi-medium nonlinear heat transfer problems*, Eng. Anal. Bound. Elem., *117* (2020), 66–75.